ISSN: 2249-7196
IJMRR/Jan 2022/ Volume 12/Issue 1/Article No-1/01-18
Capt. Mr. L. Harish / International Journal of Management Research & Review

The Impact of Liquefaction on the Behavior of Retaining Walls is Studied

[1]Mr. L. Harish, [2]Mr. B, Suresh, [3]Mr. S. Kiran Kumar, [4]Mrs. D, Anusha, [5]Mr. SK. Imran Pasha
[1,2,3,4,5] Assistant Professors, Department of Civil Engineering, Swarna Bharathi Institute of Science & Technology, Khammam – 507002, Telangana

ABSTRACT

Retaining walls constructed adjacent to underground water are the structures which may be influenced by liquefaction. The design of these structures under vibration involves determining their displacements and forces caused by earthquake and liquefaction phenomena. In this study, it is attempted to assess the effect of liquefaction on the behavior of retaining walls using finite element method (FEM). The OPENSEES software is used for this purpose, which can simulate the behavior of saturated porous media using the u-P correlation formulation. Moreover, the Dafalias-Manzari critical state two-surface plas- ticity behavioral model is applied to simulate the behavior of sand, which can model a variety of behaviors of saturated sand in various uniaxial and cyclic loadings under drained and undrained conditions for different relative densities. The results of this study suggest that the OPENSEES software and Dafalias-Manzar behavioral model possess essential capabilities for numerical modeling of behavior of retaining walls under liquefaction conditions. The presence of retaining walls also chang- es the pattern of development of excess pore water pressure, particularly at middle depths of the wall.

Key words: Retaining wall, Liquefaction, Saturated sand, Critical state.

1. INTRODUCTION

Damage to bridges, piers, deep foundations, and vital arterial highways has resulted from oil liquefaction, one of the most critical and challenging concerns in seismic geotechnics. This phenomenon results from the undrained behavior of saturated loose sandy soils under cyclic stresses. All liquefaction processes have the characteristic of an increase in pore water pressure in the absence of drainage. Rapid loading in undrained, wet sand causes the soil to compress, raising the pore water pressure and decreasing the effective stresses. Soil liquefaction happens often in previously liquefied places when ground conditions have not been altered, according to an analysis of liquefied locations. Soils that have already been liquefied are especially vulnerable to doing so again during earthquakes (1). It was once thought that liq- uefaction only occurred in sandy soils. Liquefaction has been recorded even in gravel soils under undrained conditions (1), and it was later shown that non-plastic and non-cohesive coarse- grained silt is more vulnerable to liquefaction. Liquefaction phenomenon caused extensive damage to buildings, bridges, highways, and most importantly, vital arterials, during the 1906 San Fernando earthquake. Heavy casualties and economic losses were sustained by the city as a result of the earthquake's disruption of main water supply pipelines in the city center of San Francisco owing to lateral spreading (2, 3).

Many bridges, buildings, roads, and arterials connecting Alaskan communities including Anchorage, Kodiak, Valdez, Sward, Portage, and Whittier were destroyed by lateral spreading during the 1964 Alaska earthquake. The lateral spreading phenomenon was responsible for roughly

There was a total loss of $80 million and 266 bridges (4). After reviewing the data on lateral spreading recorded in different earthquakes, researchers came to the conclusion that earthquakes are more likely to cause liquefaction-induced lateral ground movement in slopes terminating a canal, river, or excavated area; in these cases, more dis- placement typically occurs compared to when there is no pit or canal down the slope (4). Over the past 50 years, soil liquefaction has severely damaged many coastal infrastructure, especially gravity quay walls. This is why it's crucial to evaluate liquefaction potential and employ appropriate procedures for the forecasting of potential hazards. Deformations of a gravity quay wall under seismic loads were studied with a series of 1G shaking table experiments, which revealed that the bed soil significantly affects the seismic response of a gravity wall (5). A test of liquefaction and lateral spreading utilizing a viscous fluid in place of water revealed very different dis- placement profile patterns. None of the slopes of these curves changed suddenly, indicating that there was no strain concentration in the viscous fluid. In all experiments, however, pore water pressure growth and cumulative displacement ceased after the shaking stopped (6-8). Liquefiable soil, according to a quasi-plastic model used in liquefaction modeling, exhibits fluid-like behavior similar to that of a flowing quasi-plastic fluid; however, after the pore water pressure drops and the liquefied dynamic volume contracts, the soil reverts to its solid-like state. Both dynamic and static loads, as well as nonlinearity and geometry of materials, are accounted for in these universal equations. (18).

For two-phase elements, the momentum equilib- rium equation for the whole element is expressed as fol- lows (19):

1. $$div\sigma + \rho b = \rho \ddot{u_s} + \rho_f \ddot{u_{rf}}$$

where σ is the total stress, u_s and u_{rf} are the displacement of solid phase and the relative displacement of fluid phase versus solid phase, respectively, ρ and ρ_f are the density for the whole element and fluid phase, respectively, and b is the body forces. The absolute displacement of fluid phase (u_f) is calculated using the equation below:

2. refer the model to the real phenomenon and relate the flow velocity to the square root of thickness of liquefiable soil layer (9). Considering the Mohr-Coulomb model for determining the development of excess pore water pressure

in the sand under cyclic loading, it was found that the nu- merical model estimated the horizontal deformations of the wall more than actual values and predicted the vertical deformations less than measured values (10). Pile walls could mitigate structural damage in soil liquefaction condi-

where n is the porosity ratio.

If the moment equilibrium equation is considered only for fluid phase, the following equation is obtained:

$$-gradP - R + \rho\, b = \rho\, (\ddot{u} + \frac{\ddot{u_{rf}}}{n})$$

tions, resulted in a more uniform settlement in the structure (11). The studies on soil improvement against liquefaction showed that the shear probability

3.using soil-cement walls

$f \quad f\, s \quad n$

exists along the full length of the wall in large vibrations (12). The static and dynamic studies on retaining walls with liquefiable backfills demonstrated that statics is as highly important as dynamics. The measurements on the wall and its backfill showed that the specific boundary behavior, e.g. the adsorbent materials, are less important than the soil type, input flow type and embankment length, especially when it is far larger than the height of wall (13). The effect of boundary conditions and slope on soil lique- faction indicated that variation of pore water conditions is excessive in the downstream of slope (14). An evaluation of performance of cutoff walls in reducing liquefaction- induced uplift of large underground structures showed that cutoff walls prevent the deformation of liquefied soil and

high uplifts in underground structures (15). An investiga-

where P is the pore fluid pressure, R is the result of resistant forces caused by the fluid viscosity and $\ddot{u} + \frac{\ddot{u_{rf}}}{n}$ is

s

the absolute acceleration of fluid phase. In porous media, the fluid flow is usually slow and it is possible to apply theDarcy's law as follows:

4. $$\dot{u_{rf}} = kR$$

where k is the permeability tensor which can be considered $k_{ij} = k\delta_{ij}$ in homogenous

porous media. Equations 4 and 5 are combined as follows:

$$u^{\cdot} = k - gradP - R + = (u^{\cdot\cdot} + \frac{u_r^{\cdot\cdot} f}{})$$

tion into the liquefaction-induced lateral load on a pile group behind quay wall indicated that the lateral pressure on the piles near the back of the wall is much more than that on the piles farther from the wall (16, 17). Given the importance of liquefaction phenomenon in this research, the effect of liquefaction on the behavior of retaining walls is assessed using the Dafalias-Manzari critical state two- surface plasticity behavioral model.

2. RESEARCH METHODOLOGY AND MATERIALS

The moment equilibration and other aspects of the general behavior of saturated porous media are governed by the differential equations.-

Using the complete set of equations to do the analysis is both time-consuming and expensive. Simplifying the problem analysis may be accomplished in practice by eliminating those words that have a negligible impact on the outcomes, depending on the nature of the problem. For moderate-frequency occurrences like earthquakes, according to Zienkiewicz and Shiomi (1984), the relative acceleration of the fluid phase compared to the acceleration of the solid phase is minimal and insignificant. Furthermore, Chan (1988) claimed that the fluid equilibrium moment

phase, the term üs has a little influence on the outcomes and, on the other hand, causes the asymmetry of total coefficient matrix and numerical issues in the system of equations; consequently it can be omittedPutting aside the aforementioned caveats, the concluding form of equations is thus written as follows (19).

$$\frac{\partial \sigma'_{ij}}{} + \frac{\partial P}{} + pb = p\ddot{u}$$

ble to simulate the hardening and softening behaviors, body response and development of pore water pressure in loose and dense states compared to the critical state (21, 22).
The main structure of the model is based on critical state soil mechanics. The critical state, where the deformation of specimen permanently continues under constant stresses at a volumetric strain rate of zero, happens when the stress ratio ($5 = \frac{q}{p}$) equals the critical stress ratio (M) and the void ratio (e) equals its critical limit (e_c). The critical void ratio is just a function of effective confining pressure known as the critical state line (CSL). This equation is usually used in a logarithmic form, but its exponential form is considered in this model. According to Li and Wang (1998), the exponential equation is valid in a broad-

Obviously, the number of equations is thus reduced from 3 to 2. These equations are abbreviated to $u - P$ formulation. In this study, this formulation is used to model the behavior of saturated porous medium. The matrix formulation of $u - P$ equations is obtained using finite element method

er range of confining pressures (23). The equation applied for the CSL in this model is as

follows (21):

10. $e_c = e_0 - \lambda_c \left(\frac{P_c}{P_{at}}\right)^{\xi}$

9. $M\ddot{U} + \int_V B^T \sigma' dV - QP - f^{(s)} = 0$

where e_0, λ_c and ξ are the parameters of the model and P_c and P_{at} are the confining pressure and atmospheric pres- sure, respectively.

In this model, the soil behavior is determined in terms of the distance from the critical state. The state parameter is used for this purpose, defined as follows (21):. $Q^T\dot{U} + HP + S\dot{P} - f^{(p)} = 0$

11. $\psi = e - e_c$

where e and e_c are the current and critical void ratios, re-

where M is the mass of the system, B is the strain- displacement matrix, Q is the correlation matrix for both equations, S is the compatibility matrix and H is the per- meability matrix. Vectors $f^{(s)}$ and $f^{(p)}$ include all effects of body and surface forces defined in the boundaries.

The results of Taiebat et al (2007) showed that boundary surface models are so useful to model liquefaction phe- nomenon and liquefaction-induced settlements (20). How- ever, the model proposed by Dafalias and Manzari (2004) possessed more abilities than previous boundary surface models and could simulate the behavior of sand under uni- form and cyclic loadings in drained and drained conditions (21). Thus, this behavioral model is used in this study to model the behavior of saturated sand. The formulation of this model is based on the boundary surface plasticity in the space relative to deviator stresses in the framework of critical state soil mechanics. In this model, the relationship between the major and minor stress ratio and the ratio of dilation stress to critical stress is determined by the state parameter. The state parameter represents the distance be- tween the current state of soil element and the critical state line (CSL). When this parameter is used in the formulation of model, it is possible to model the behavior of a type of sand for different densities under different confining pres- sures using a set of constant parameters. Hence it is possi-

spectively, defined for the same confining pressure. In the model proposed by Dafalias and Manzari (2004), this pa- rameter is used to define the boundary stress and dilatancy stress ratios (21):

12. $M^d = M\ e(n^d\psi)$

$M^b = M \exp(-n^b\psi)$

13.

where M, M^b and M^d are the critical stress, peak stress and dilatancy stress ratios, respectively, and n^b and n^d are the constants of the model. In this model, the dilatancy line is the same as phase change line proposed by Ishihara et al (1975) (24). A function in terms of modified Lode angle ( ) is used to generalize these equations to the three-dimensional stress space (generalization of line to surface). Figure 1 schematically shows the critical, peak and dila- tancy surfaces in the surface π. When the critical, peak and dilatancy surfaces are determined, the equations of the behavioral model can be defined (21).

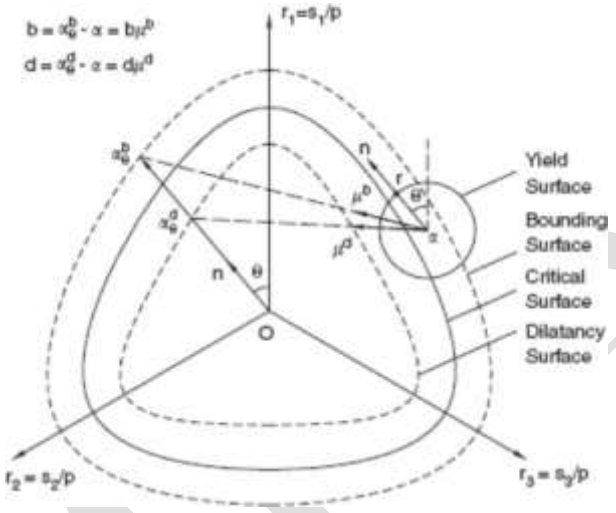

Figure 1. Schematic illustration of Manzari and Daralias model (2004) in surface π (21)

The differential equations should be integrated in the range of time to complete the numerical solution. There are a variety of methods for this purpose. These methods may be either multi-step or single-step. Two identical but inde- pendent categories are developed for single-step methods. The first category is based on residual weight and finite element in the time range, while the second category is based on the generalization of Newmark method or finite differences (25). In this study, the single-step method is utilized to solve moment equations. Given the method above, the error of moment equilibrium equation is limited to the maximum allowable error, as expressed below:

14. $R_{t+\Delta t} = F - M\ddot{U}_{t+\Delta t} - C\dot{U}_{t+\Delta t} + F(U_{t+\Delta t})^{int}$

The values of $U_{t+\Delta t}$ and $\dot{U}_{t+\Delta t}$ are determined using the Taylor series as follows:

Differential equations regulate the moment equilibration and the overall behavior of saturated porous media.

It takes a lot of time and resources to perform the analysis using the full set of equations. Depending on the specifics of the situation at hand, cutting out terms that don't make much of a difference in the results can be a practical way to simplify the analysis. According to Zienkiewicz and Shiomi (1984), the relative acceleration of the fluid phase compared to the acceleration of the solid phase is small and negligible for events that occur with moderate frequency, such as earthquakes. Not only that, but the fluid equilibrium moment is said to

phase, the term üs has a small impact on the results and, on the other hand, causes the asymmetry of total coefficient matrix and numerical difficulties in the system of equations; thus it may be omitteIgnoring the aforementioned qualifiers, the final form of

15. $U_{t+\Delta t} = U_t + \Delta t U$

16. $U_{t+\Delta t} = U_t + \Delta t U_t \pm$

2

The equations are re-written by converting newton:

equilibrium equations must be solved by correlation. Moreover, more accurate behavioral models, e.g. Dafalias-Manzari model (2004), should be utilized for more precise modeling of soil behavior. Given the requirements, the19. $U_{t+\Delta t} = U_t + \Delta t \dot{U}_t + [(0.5-\beta)\Delta t^2 \ddot{U}_t + \beta \Delta t^2 \ddot{U}_{t+\Delta t}$

20. $\dot{U}_{t+\Delta t} = \dot{U}_t + [(1-\gamma)\Delta t]\ddot{U}_t + [\gamma \Delta t]\ddot{U}_{t+\Delta t}$

(29). In this study, the results achieved by Maharjan and Takahashi (2013) are employed to validate the numerical model. Maharjan et al prepared four specimens for centri- fuge tests to investigate the impact of silt layers with lower permeability between sand layers. The tests are done on a scale of 40:1. The specimens are made in a shear box measuring 500 mm × 200 mm × 450 mm, which corre- sponds to a sand deposit 9.8 m in height on prototype scale. The Toyoura sand is used for these tests. The soil proper- ties are listed in Table 1. The sand specimens are prepared

at relative densities of 50-55% using sand pluviation tech- nique and there are two silt layers 1 m in height in the se-

cond specimen (on prototype scale) (30).**Table 1. Soil properties for tests by Maharjan (31)**

Property	*Toyoura sand*
G_s	2.65
$D_{50}(mm)$	0.19
$D_{10}(mm)$	0.14
e_{max}	0.973
e_{min}	0.609
Permeability $k(m/s)$	$2 \times 10^{-}$
sand %	100%

Table 2 also presents the parameters of behavioral model used in this study.

Table 2. Parameters of Manzari's behavioral model for Toyoura sand (30)

Amount	*Parameter symbol*	*Parameter performance*
125	$G_0(kPa)$	Elastic
0.05		
1.25	M	Critical state
0.712	c	
0.019	λ_c	
0.934	e_c	
0.7	ξ	
0.01	m	Yield surface
0.704	A_0	Dilatancy
3.5	n^d	
7.05	h_0	Modulus of plasticity
0.968	c_h	

4	1.1 600	n^b_{zmax} c_z	Fabric tensor

In these tests, the sand layer is completely saturated and the model is rotated at an acceleration of 40g and then vi- brated horizontally. The input horizontal acceleration of

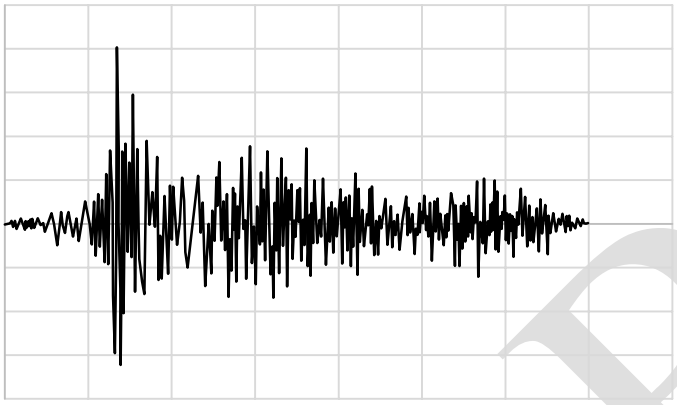

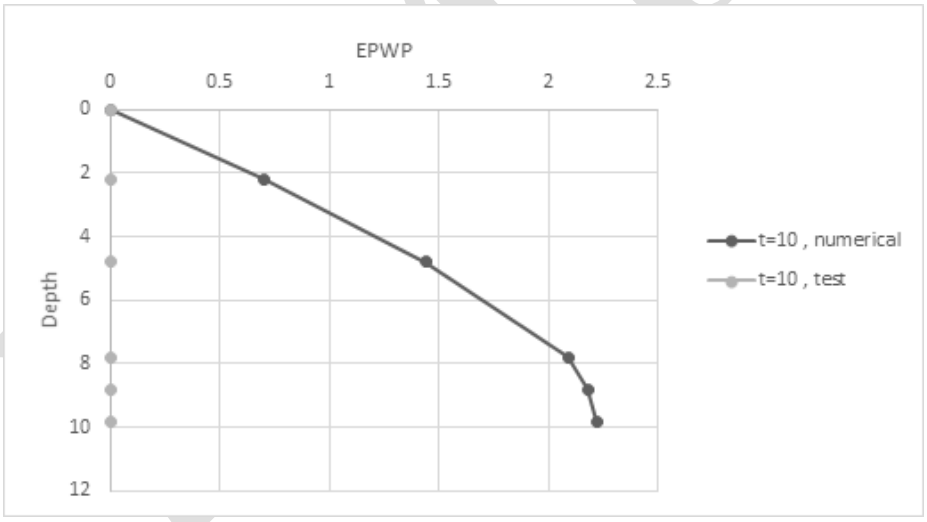

Figure 3. Excess pore water pressure at 10 sec

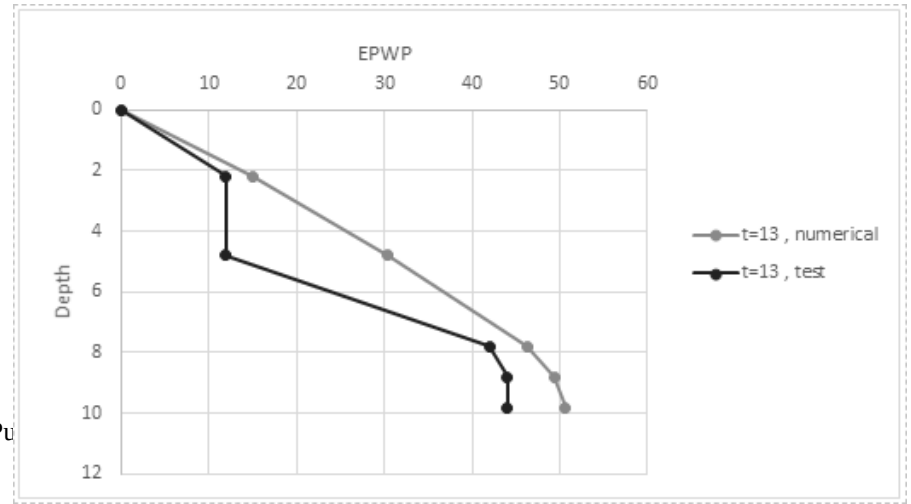

Figure 4. Excess pore water pressure at 13 sec

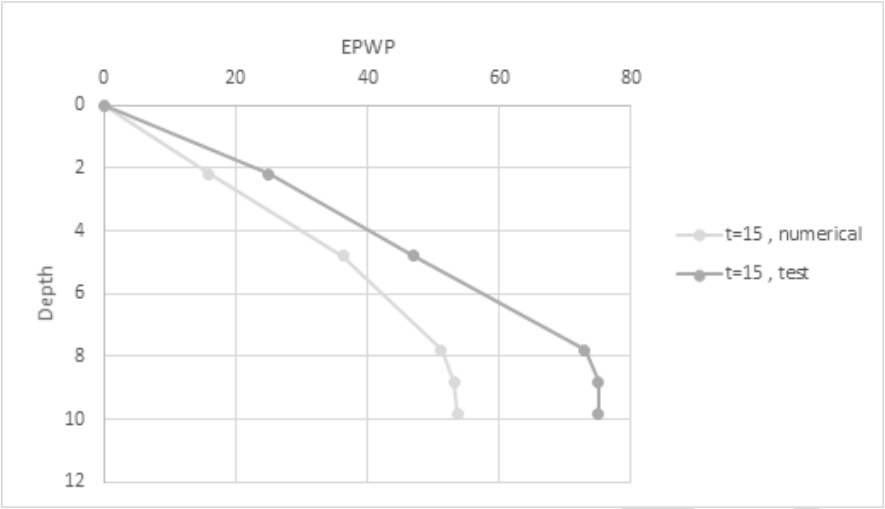

Figure 5. Excess pore water pressure at 15 sec

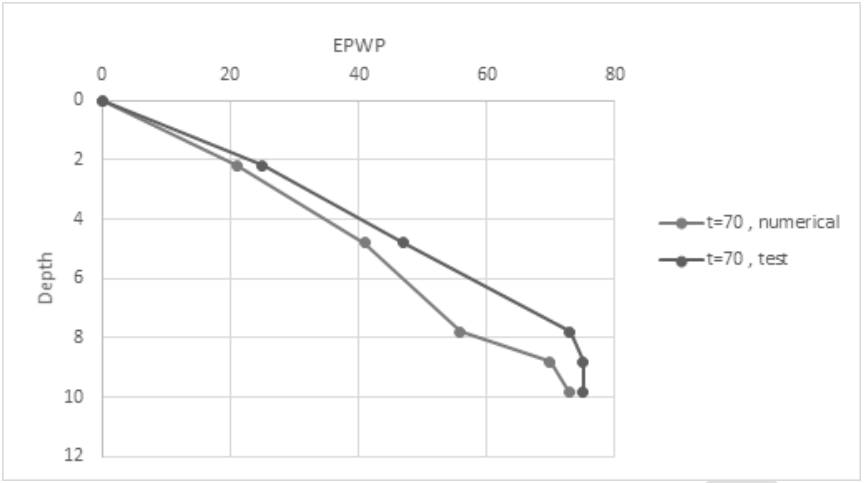

Figure 6. Excess pore water pressure at 70 sec

An investigation of the results suggests that there is good agreement between the results of excess pore water pres- sure at different depths for numerical and experimental modelings. Figure 7 also shows the liquefaction-induced displacements of ground surface for numerical and exper- imental modelings.

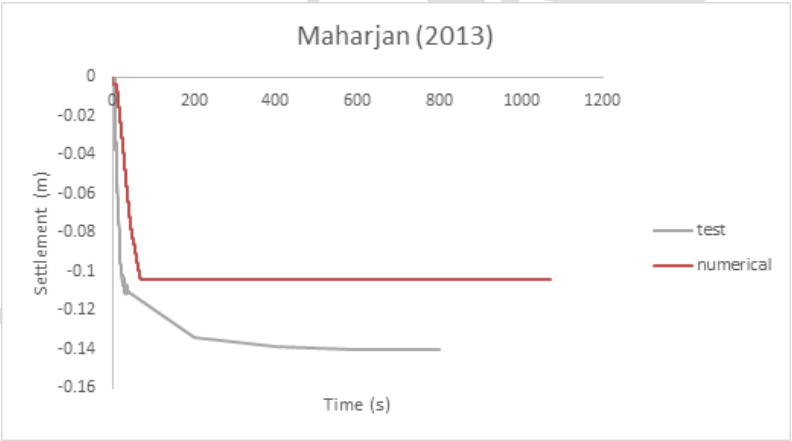

Figure 7. Ground surface settlement

Liquification and subsequent consolidation are depicted in this flowchart. Because of the intricacy of the liquefaction phenomena, this figure shows that there is an acceptable gap of roughly 25% between the findings of nu- merical and experimental modelings. To evaluate the impact of liquefaction on retaining walls (31), this work used numerical modeling of the VELACS11 test to analyze the behavior of a gravity pier situated in saturated sandy soil. At Cambridge, they are now carrying out the VELACS11 centrifuge test. A 0.478-meter-long metal component with a 0.10-by-0.05-meter cross section serves as a gravity pier in this model's wet sand layer. To ensure that all of the water in the backfill drains properly, a lead load 0.002 m thick and 0.48 m broad is put at a distance of 0.01 m above it. This lead sheet is 0.48 centimeters in width and 1 meter in length. At this point, the water is only 0.01 meters over the sand (31). The testing chamber is 0.9 m 0.48 m 0.22 m and has a stiff, inflexible, flat surface and bottom. After thoroughly soaking the sand layer, the model is spun at a centrifugal acceleration of 50g, and the test box is horizontally vibrated in its base. With a maximum amplitude of 0.25g and a frequency of 1.92 Hz at full scale, the input horizontal acceleration has a roughly sinusoidal profile. The test's input acceleration time history (31) is depicted in Figure 8.

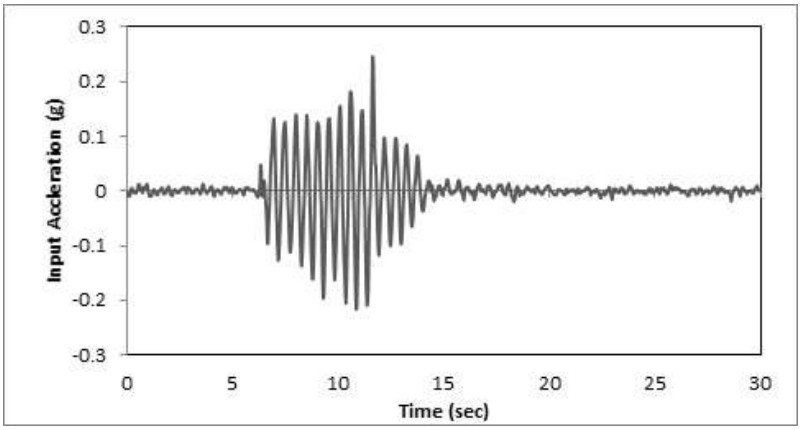

Figure 8. Input acceleration time history for VELACS11 model (31)

The Nevada sand is used at a relative density of 60% in this test. Table 3 shows the mechanical and hydraulic

properties of the sand, aluminum and lead used in this test.

Table 3. Mechanical properties of Nevada sand at relative density of 60% (31)

0.400	Porosity (n)	Nevada sand with D=60%
15.76	Dry unit weight (KN/m^3)	
$5.6_5 \times 10$	Permeability coefficient (m/s)	
$2.8_3 \times 10$	Permeability coefficient on full scale (m/s)	
27.16	Unit weight (KN/m^3)	Aluminum
7.0×10^7	Young modulus (KN/m^2)	
0.33	Poisson ratio	
$1.0_9 \times 10$	Permeability coefficient (m/s)	
110.81	Unit weight (KN/m^3)	Lead

In the modeling of this test, the Manzari-Dafalias model is used to predict the behavior of saturated sand and the alu- minum wall is modeled using the elastic behavioral model. The effect of lead plate is considered along a 5 m distance from the surface of backfill under undrained condition and its rigidity is neglected. In the modeling, 4-node rectangu- lar elements are applied for deformations and all nodes of the element have the degree of freedom of pore water pres-sure. The wall nodes are connected to the backfill nodes through EDF command and the relative displacement be- tween the soil and the wall is ignored. The parameters of Nevada sand are listed in Table 4. These parameters are calibrated.

Table 4. Parameters of behavioral model for Nevada sand (31)

Amount	*Parameter symbol*	*Parameter performance*
150	$G_0(kPa)$	Elastic
0.05		
1.14	□	Critical state
0.78	□	
0.027	□□	
0.83	□□	
0.45	□	
0.02	□	Yield surface

0.81	$\sqcup_0$	Dilatancy
1.05	$\square\square$	
9.7	h_0	Modulus of plasticity
1.02	$\sqcup_h$	
2.56	$\square\square$	
5	$\sqcup\square\square\square$	Fabric tensor
800	$\square_\square$	

In the modeling process, a model is initially made under static conditions. Horizontal in situ stresses are calculated by $\square_0$ = 0.2. Then, each calculated in situ stress is used in the dynamic analysis as an initial stress condition. It is worth mentioning that various values of $\square_0$ are evaluated to examine the effect of lateral in situ stresses on the be- havior of retaining wall; eventually, it is found that the impact of this parameter on the wall behavior is negligible in numerical modeling. Given the analyses conducted to determine appropriate time step for obtaining the most

accurate solution and high sensitivity of this problem to the selected time step, the time step of $\Delta\square$ = 0.002 □□□ is em- utilized for the research's computations. The correctness of the flow and equilibrium equations, as well as the trustworthiness of the findings, are all profoundly affected by the chosen time step. It should be noticed that the output values are not consistent with the test results since the time step of t = 0.002 sec is initially utilized for modeling this test. Therefore, sensitivity analysis or some other method must be used to establish the appropriate time step in each simulation.

alternative current techniques, such that stability condition and calculation accuracy are fulfilled and the time spent on calculations and analysis is maintained to a minimum. To arrive at a numerical solution, the differential equations are integrated over the relevant time interval. In this case, we use the Newmark technique of generation of finite differences.

RESULTS, DISCUSSION AND EVALUATION

Figure 9 illustrates the liquefaction-induced permanent horizontal displacement of the wall measured by the dis- placement meter during the test conducted at Cambridge University and It is observed that the process of lateral displacement of the wall is relatively compatible with the results of VE- LACS11 centrifuge test, but the values of numerical mod- eling are lower than those recorded for the test. The differ- ences in numerical and experimental modelings may be due to the parameters applied in the Manzari-Dafalias

model to predict the behavior of saturated sand and the impossibility of accurate modeling of pier structure in con- tact with the soil. Figure 10 demonstrates the liquefaction- induced permanent horizontal displacement of the wall using numerical modeling.

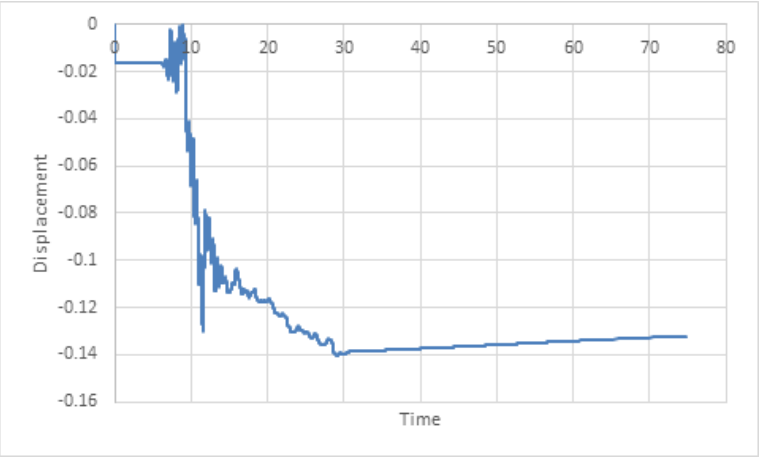

Given the lack of results of physical modeling, it is not possible to compare the results directly. However, the fig- ure reveals a 14 cm liquefaction-induced settlement in the backfill, which may cause serious damage to the backfill structures. Figure 11 shows the excess pore water pressures

during the test at Cambridge University and the values predicted by numerical modeling using the Manzari- Dafalias model.Modeling and experimental data from a pore water pressure meter show a show a marginal deviation from maximum pore water pressure, which might be due to the inaccuracies inherent in current methods for predicting how liquefied sand would behave under low effective stresses and associated restrictions. Differences in pore water pressure dissipation may be attributable to a number of factors, including the permeability and draining velocity of the water used in the studies. There is also a good agreement between the test findings and the numerical modelings of the development process of pore water pressure when the input acceleration and projected maximum pressure are applied. However, the maximum pore water pressure and its change can be predicted with reasonable accuracy, given the variance of excess pore water pressure at P4, something the numerical model cannot achieve. Numerical modeling cannot anticipate pore water pressure and suction in the backfill, as evidenced by the variations in P5's excess pore water pressure. Possible factors include the challenge of anticipating the suction state and the inaccuracy of the simulation of the pier structure and sand. There is only around a 20% discrepancy between the calculated maximum pore water pressure and the experimental results. This is also shown in the P6 pore water pressure and may be attributable to the model's lack of accuracy in predicting the complex soil behavior that is simultaneously impacted by factors such wall displacement and impermeability, the displacement of liquefied soil, and the weight of the soil. and lead plate's impermeability, given that it's in aWalls 7 and 8 m in height show horizontal displacement in Figure 12a,b, with crest horizontal displacements of 25 cm and 28 cm, respectively, which might lead to extensive failures of structures embedded in the backfill.

Assessing the excess pore water pressure for the wall 8 m in height, it is found that the maximum effect

of the wallon excess pore water pressure occurs at a depth of 4 m, while this effect is far less at a depth of 8 m, i.e. the bottomof the wall.

3. CONCLUSION

1. Numerical methods implemented inside OpenSees finite element software are used to assess the effects of liquefaction and lateral spreading on coastal structures in this investigation. The u-P correlated formulation regulating saturated porous media is used in the numerical model, which treats soil mass as a continuous medium to account for the correlation between the solid and fluid phases. To better characterize the seismic behavior of saturated sand during liquefaction, the idea of variable permeability is utilized to more precisely estimate the settlement and lateral displacement, as well as to anticipate the rate of formation and dissipation of pore water pressure. The following are the study's findings:
2. 1. The modeling accurately depicts the earthquake-vulnerability of pier and gravity quay structures, highlighting the significance of revising design norms and standards for the purpose of reducing failures.
3. Second, the liquefaction-induced lateral displacement of the wall is reasonably comparable with the findings of VELACS11 centrifuge tests in the numerical modeling of VELACS11 test. Possible causes of discrepancies between numerical and experimental models include the use of different sand parameters in the Manzari-Dafalias model and the difficulties of accurately predicting the pier construction.
4.
5. 3. The growing trend of pore water pressure under input acceleration and the dissipation of pore water pressure at zero acceleration are appropriately compatible with the findings of centrifuge tests in the numerical modeling of VELACS11. The inability of the methods used for accurate modeling of the behavior of liquefied sand under low effective stresses, the im- possibility of accurate modeling of the pier structure in the VELACS11 test, the boundary conditions of the test box, and similar rules in centrifuge tests all contribute to discrepancies between the numerical and experimental modelings of changes in porewater pressure. Errors in modeling wall lateral displacement can amplify these errors in predicting pore water pres- sure because of the influence of velocity and wall displacement on the pore water pressure developed in the backfill.
6. Suction in the backfill arises as a result of horizontal displacement in the static analysis, leading to pore water pressure oscillations.
7. When it comes to the stability condition being met and the precision of your predictions, the time step you choose makes a big difference. equilibrium and flow equations and reliability of results; so the time step of $\Delta\square = 0.002$ The VELACS11 simulation utilizes sec. at ensure stability and calculational correctness while keeping analytical calculations and time at a tolerable level, the appropriate time step in each model must be determined by sensitivity analysis or other available approaches.

   The surplus pore water pressure decreases at a certain depth as the distance from the retaining wall rises. The effect is amplified closer to the wall's center.

REFERENCES

1. Kramer SL. Performance-based design methodologies for geotechnical earthquake engineering. Bulletin of Earthquake Engineering. 2014;12(3):1049-70.
2. Baska DA. An analytical/empirical model for prediction of lateral spread displacements. 2003.
3. Naseri F, lotfollahi S, Bagherzadeh khalkhali A. Dynamic Mechanical Behavior of Rock Materials.

Journal of Civil Engineering and Materials Application. 2017;1(2):39-44.
4. Youd TL, Perkins DM. Mapping of liquefaction severity index. Journal of Geotechnical Engineering. 1987;113(11):1374-92.
5. Ghalandarzadeh A, Orita T, Towhata I, Yun F. Shaking table tests on seismic deformation of gravity quay walls. Soils and foundations. 1998;38(Special):115-32.
6. Taboada V, Abdoun T, Dobry R, editors. Prediction of liquefaction-induced lateral spreading by dilatant sliding block model calibrated by centrifuge tests. Proc, 11th World Conf on Earthquake Engineering; 1996: Pergamon Oxford, UK.
7. Gonzalez L, Abdoun T, Sharp MK. Modelling of seismically induced liquefaction under high confining stress. International Journal of Physical Modelling in Geotechnics. 2002;2(3):01-15.
8. Tamate S, Towhata I. Numerical simulation of ground flow caused by seismic liquefaction. Soil Dynamics and Earthquake Engineering. 1999;18(7):473-85.
9. Hadush S, Yashima A, Uzuoka R. Importance of viscous fluid characteristics in liquefaction induced lateral spreading analysis. Computers and Geotechnics. 2000;27(3):199-224.
10. Byrne PM. A model for predicting liquefaction induced displacement. 1991.
11. Sáez E, Ledezma C. Liquefaction mitigation using secant piles wall under a large water tank. Soil Dynamics and Earthquake Engineering. 2015;79:415-28.
12. Boulanger RW, Khosravi M, Khosravi A, Wilson DW. Remediation of liquefaction effects for an embankment using soil-cement walls: Centrifuge and numerical modeling. Soil Dynamics and Earthquake Engineering. 2018;114:38-50.
13. Dewoolkar M, Ko H-Y, Pak R. Experimental developments for studying static and seismic behavior of retaining walls with liquefiable backfills. Soil Dynamics and Earthquake Engineering. 2000;19(8):583-93.
14. Hung W-Y, Lee C-J, Hu L-M. Study of the effects of container boundary and slope on soil liquefaction by centrifuge modeling. Soil Dynamics and Earthquake Engineering. 2018;113:682-97.
15. Liu H, Song E. Working mechanism of cutoff walls in reducing uplift of large underground structures induced by soil liquefaction. Computers and Geotechnics. 2006;33(4-5):209-21.
16. Liu C, Tang L, Ling X, Deng L, Su L, Zhang X. Investigation of liquefaction-induced lateral load on pile group behind quay wall. Soil Dynamics and Earthquake Engineering. 2017;102:56-64.
17. Tang L, Ling X, Zhang X, Su L, Liu C, Li H. Response of a RC pile behind quay wall to liquefaction-induced lateral spreading: a shake-table investigation. Soil Dynamics and Earthquake Engineering. 2015;76:69-79.
18. Alyami M, Rouainia M, Wilkinson S. Numerical analysis of deformation behaviour of quay walls under earthquake loading. Soil Dynamics and Earthquake Engineering. 2009;29(3):525-36.
19. Zienkiewicz OC, Chan A, Pastor M, Schrefler B, Shiomi T. Computational geomechanics: Citeseer; 1999.
20. Taiebat M, Shahir H, Pak A. Study of pore pressure variation during liquefaction using two constitutive models for sand. Soil Dynamics and Earthquake Engineering. 2007;27(1):60-72.
21. Dafalias YF, Manzari MT. Simple plasticity sand model accounting for fabric change effects. Journal of Engineering mechanics. 2004;130(6):622- 34.
22. Biot MA. Theory of propagation of elastic waves in a fluid-saturated porous solid. II. Higher frequency range. The Journal of the acoustical Society of america. 1956;28(2):179-91.
23. Li X-S, Wang Y. Linear representation of steady-state line for sand. Journal of geotechnical and geoenvironmental engineering. 1998;124(12):1215-7.
24. Ishihara K, Tatsuoka F, Yasuda S. Undrained deformation and liquefaction of sand under cyclic stresses. Soils and foundations. 1975;15(1):29-44.
25. Newmark NM. Effects of earthquakes on dams and embankments. Geotechnique. 1965;15(2):139-60.
26. Newmark NM. A method of computation for structural dynamics. ASCE J Eng Mech div. 1959;85:67.
27. Das BM, Sobhan K. Principles of geotechnical engineering: Cengage learning; 2013.
28. Helal AA. Axially loaded pile behavior in sands with/without limited liquefaction: The University of Alabama in Huntsville; 2012.
29. OpenSees MF. Open system for earthquake engineering simulation. Pacific Earthquake Engineering

Research Center, University of California …; 2013.
30. Maharjan M, Takahashi A. Centrifuge model tests on liquefaction-induced settlement and pore water migration in non-homogeneous soil deposits. Soil Dynamics and Earthquake Engineering. 2013;55:161-9.
31. Shahir H, Pak A, Taiebat M, Jeremić B. Evaluation of variation of permeability in liquefiable soil under earthquake loading. Computers and Geotechnics. 2012;40:74-88.